Available online at www.sciencedirect.com
SCIENCE DIRECT
Journal of Catalysis 228 (2004) 192–205
JOURNAL OF CATALYSIS
www.elsevier.com/locate/jcat

Isopropylation of benzene with 2-propanol over AFI aluminophosphate molecular sieves substituted with alkaline earth metal

Suresh B. Waghmode [1], Shyamal Kumar Saha [2], Yoshihiro Kubota [3], Yoshihiro Sugi *

Department of Materials Science and Technology, Faculty of Engineering, Gifu University, Gifu, 501-1193, Japan

Received 14 February 2004; revised 2 June 2004; accepted 21 July 2004

Available online 11 September 2004

Abstract

Aluminophosphate ($AlPO_4$-5) molecular sieves partly substituted with alkaline earth metal in the framework (MAPO-5; M = Mg, Ca, Sr, and Ba) have been employed as catalysts for the isopropylation of benzene with 2-propanol. The incorporation of alkaline earth metal ions gives rise to Brønsted acidity of different acidic strengths. The influence of type of alkaline earth metals, MO/Al_2O_3 ratio, reaction parameters such as reaction temperature, molar ratio of benzene and 2-propanol (B/IP), space velocity, and time on stream were studied. The selectivity of cumene (IPB) and benzene conversion was in the order Mg ≫ Ca > Sr > BaAPO-5. This order is correlated with acidity of the molecular sieves. The selectivity of IPB for MgAPO-5 was maximized at $MgO/Al_2O_3 = 0.1$. It increased with reaction temperature, low WHSV, high B/IP ratio, whereas it decreased with time on stream. The major by-products were 1,3- and 1,4-diisopropylbenzenes (1,3- and 1,4-DIPBs): among them, 1,3-DIPB was predominant over 1,4-DIPB at higher temperatures. The dealkylation of 1,3- and 1,4-DIPBs gives IPB as a major product. Molecular modeling studies reveal that 1,3-DIPB is the most stable and bulkier among DIPB isomers.

Keywords: MAPO-5; Acidity; Isopropylation; IPB selectivity; DIPB; Diffusion; Molecular modeling

1. Introduction

Cumene (IPB) is an important commodity in petrochemicals, mainly used for the production of phenol and acetone, which are again processed with other chemicals to produce resins, plastics, and other value-added products such as hydroquinone and resorcinol [1]. In recent years, more than 90% of phenol is produced from IPB. It has been expected that the world's demand of IPB will increase by ∼ 3.5% per year over the next 5 years [2]. Different types of solid acids have been investigated to synthesize IPB, and acidic zeolites are found as the most suitable catalysts. Shape-selective alkylation of benzene and toluene over zeolite catalysts has been extensively studied [1–6]. Their use in commercial processes has been sought only recently by Mobil, Dow, CD Tech., UOP, and Enichem for the production of IPB (based on MFI, BEA, MCM-22, MOR, FAU, etc.) [3]. Synthesis of IPB by the alkylation of benzene with 2-propanol or propene has been reported in the literature [4–19]. Recently, Das et al. reported a sulfated ZrO_2–TiO_2 catalyst for the isopropylation of benzene with 2-propanol [20].

Mild acidity is required for the alkylation of benzene with 2-propanol or propene over zeolites [21]. A new family of aluminophosphate molecular sieves (abbreviated as AlPOs) has drawn considerable attention [22]. However, there have been only few a reports on catalytic research of aluminophosphates such as $AlPO_4$-5. The main disadvantage is the mild acidic nature of AlPOs. Considerable effort has been directed toward isomorphous substitution of Al and or P by other elements in the framework to generate Brøn-

* Corresponding author. Fax: + 81-58-293-2597.
E-mail address: sugi@apchem.gifu-u.ac.jp (Y. Sugi).
[1] Current address: Departement of Chemistry, University of Pune, Pune 411007, India.
[2] Current address: Department of Chemical Technology, College of Engineering, Chonnam National University, Gwangju 500-757, Korea.
[3] Current address: Division of Materials Science and Engineering, Graduate School of Engineering, Yokohama National University, Yokohama 240–8501, Japan.

0021-9517/$ – see front matter
doi:10.1016/j.jcat.2004.07.025

sted acid sites [23]. The acidity of the AlPOs can be modified by isomorphous substitution of alkaline earth and transition metals [24]. It has been shown that the incorporation of divalent metal ions to AlPOs improves their Brønsted acidity and increases the potential of these materials as a solid catalyst [24,25]. $AlPO_4$-5 molecular sieves partly substituted alkaline earth metal is a promising microporous material for acid catalysis.

The present study involves the synthesis of MAPO-5 molecular sieves, and vapor-phase isopropylation of benzene with 2-propanol. Molecular fitting was examined to analyze the size and shape of the molecules as well as their fitting inside 12-membered rings (12-MR) of MAPO-5. Studies on diffusion of these molecules were also carried out inside 12-MR channels of MAPO-5.

2. Experimental

2.1. Synthesis of MAPO-5 molecular sieves

The syntheses of MAPO-5 were carried out by the vapor-phase transport (VPT) method [26]; a typical gel composition was as follows: 1.0 Al_2O_3–0.10 MO–1.0 P_2O_5–0.76 Et_3N–45 H_2O.

Typical procedures are shown for the synthesis of MgAPO-5: aluminum isopropoxide (2.05 g, 5.0 mmol) was slurred in water (1.85 g). To this slurry, 85% phosphoric acid (1.15 g, 5.0 mmol) diluted in water (2.00 g) was added dropwise over a period of 0.5 h with constant magnetic stirring. Magnesium acetate (0.107 g, 0.5 mmol) was added to the resulting solution, and magnetic stirring was continued further for 1 h. The hydrogel was dried at 80 °C in an oil bath with continuous stirring to evaporate water. When the gel became thick and viscous, it was homogenized manually using a Teflon-rod until it dried. The drying period was varied (ca. 0.75–1 h) with the gel composition. A white solid formed and was then ground to a fine powder and finally transferred in a small Teflon cup (20 mm × 20 mm i.d.). This cup was placed in a 23-ml Teflon-lined autoclave with the support of a Teflon holder. Small amounts (0.3 g per 1.0 g of dry gel) of water and triethylamine (0.384 g, 3.8 mmol) were taken at the bottom of the autoclave in such a manner that no external bulk water came into the direct contact with the dry gel. The autoclave assembled for the DGC method was shown in our previous paper [26]. The crystallization was carried out at 175–200 °C in an oven under autogenous pressure for 12–24 h. The products were collected centrifugally, washed with distilled water, and dried at 100 °C overnight. The as-synthesized molecular sieve was placed in a muffle furnace and heated in air stream (flow rate: 50 ml/min). The temperature was raised from room temperature to 550 °C at 1.3 °C/min and kept at that temperature for another 7 h, and finally the sample was cooled to room temperature under ambient conditions.

2.2. Catalytic reactions

2.2.1. Isopropylation of benzene

The isopropylation of benzene with 2-propanol and the isomerization of 1,3- and 1,4-DIPBs were carried out under vapor phase using a fixed-bed down-flow reactor (Pyrex glass; 25 cm length and 1 cm internal diameter) equipped with preheater assembly. Fresh catalyst (1.0 g) was sieved (mesh size around 30) and sandwiched between glass wool plugs placed in the middle of the reactor. The reactor was heated to the requisite temperature, and the temperature of the preheater assembly was kept at 175 °C. The catalyst was activated in O_2 (50 ml/min) at 550 °C for 6 h, and the reaction was carried out at atmospheric pressure in N_2 gas flow (10 ml/min). Benzene and 2-propanol were passed over the catalyst in a ratio (B/IP) of 6. The products were passed through a water-cooled condenser, and liquid products were collected time to time after an interval of 2 h. After taking a series of data, the catalyst was reactivated in O_2 (50 ml/min) at 550 °C for 6 h for further reaction studies.

The products were identified using GC-MS (Shimadzu QP 5000) and analyzed by a Shimadzu Model 18A chromatograph (Ultra-1 capillary column (25 m × 0.3 mm)). The yield of products was calculated on the basis of benzene and 2-propanol.

2.2.2. Cracking of IPB and 1,3,5-TIPB

The catalytic activity of cracking of IPB and 1,3,5-triisopropylbenzene (1,3,5-TIPB) was carried out at 450 °C in nitrogen stream by a conventional pulse-type reactor, and products were analyzed by a Shimadzu GC-4C online gas chromatograph.

2.3. Characterization

The phase purity and the crystallinity of the sample were determined by powder X-ray diffraction with Cu-K_α radiation ($\lambda = 1.5418$ Å) using a XRD-6000 (Shimadzu Corporation). Elemental analysis was performed by inductively coupled plasma emission spectroscopy (ICP) using a JICP-PS-1000UV (Leeman Labs Inc.). The crystal size and morphology of the sample were examined by scanning electron microscopy (SEM) using a XL30 microscope (Philips). Nitrogen adsorption measurements were carried out on a BELSORP 28SA (Bel Japan). Acidity measurements were performed by temperature-programmed desorption of ammonia (NH_3-TPD) on a BEL TPD-66 (Bel Japan). FT-IR spectra in the framework region were recorded by a KBr pellet technique using 0.5 mg of sample and 100 mg of KBr on a Thermo Nicolet Nexus 470. Unit cell parameters of the samples were calculated by using the TREOR 90 program of Material Studio software supplied by Accelrys Inc. using a Dell PC (Dimension 8250 series). Pyridine adsorption on acid sites of the MAPO-5 was investigated by FT-IR spectroscopy. The sample (ca. 28 mg) was pressed into self-supporting wafers and placed into the FT-IR cell, allowing

Table 1
Dimensions, total energies, and HOMO-LUMO gap of different organic molecules in their minimum energy configuration optimized by DFT, and diffusion energy barrier in AFI ($AlPO_4$-5) molecular sieves

Molecules	Dimensions ($a \times b \times c$) (nm)	Total energy (DMol) (kcal/mol)	HOMO-LUMO gap (kcal)	Energy barrier (kcal/mol)
Propene (**1**)	$0.5 \times 0.36 \times 0.24$	−74012.5046	172.1732	1.944
Benzene (**2**)	$0.60 \times 0.53 \times 0.15$	−145778.7317	155.4999	2.544
IPB (**3**)	$0.80 \times 0.53 \times 0.52$	−219808.0539	146.5264	3.525
1,2-DIPB (**4**)	$0.75 \times 0.68 \times 0.52$	−293831.1663	146.5264	9.483
1,3-DIPB (**5**)	$0.98 \times 0.60 \times 0.52$	−293842.4419	146.2879	4.478
1,4-DIPB (**6**)	$0.10 \times 0.53 \times 0.52$	−293837.5563	144.2045	1.946
1,3,5-TIPB (**7**)	$0.96 \times 0.88 \times 0.52$	−367874.2284	144.8070	14.586

heating under vacuum. Prior to adsorption of pyridine, the sample was evacuated to ca. 10^{-3} Pa at 400 °C for 2 h, and then, cooled to 150 °C. Nearly 1.3×10^2 Pa of pyridine was introduced into the FT-IR cell. After 1 h of adsorption, the excess and weakly adsorbed pyridine was removed by evacuation at the same temperature for 1.5 h. FT-IR spectra of chemisorbed pyridine were recorded using a JEOL JIR-7000 spectrometer.

2.4. Methods and models for molecular fitting

Several zeolites have been tried experimentally for this reaction. Much attention has been focused on BEA and MCM-22 due to its high activity and predominant shape selectivity. The unique 12-member ring channel system in AFI has been used to find the cause of shape selectivity. However, aluminophosphate molecular sieves are not used as catalysts, due to low acidity. The catalytic behavior of most of the zeolites arises from the catalytically active Brønsted acid sites. These active sites are located inside the pore structures. In such cases molecular modeling and graphics can provide a better understanding of the active sites. The computational studies reported here were carried out using Material Studio's (MS) supplied by Accelrys Inc., UK. The force field energy minimization calculations were done with the Discover program to search most favorable and unfavorable adsorption of guest molecules inside hosts (zeolites) for shape-selective diffusion, using the consistent valence force field (CVFF) of Hagler et al. [27] and the parameters were obtained from the reports of Dauber-Osguthorpe et al. [28]. The detailed methodology is reported elsewhere [29]. Molecular Graphics (MG) displays were obtained from the MS system using a Dell 8250 computer.

Quantum chemical calculations for full geometry optimization of organic molecules were done with the use of modern electronic structure methodology based on the density-functional theory (DFT) by using Gaussian03 software. The total energies of the organic molecules were calculated using level 6-311G (d,p) basis sets. As exchange functional, Becke's hybrid exchange B3 was used and as correlation functionals, the Lee–Yang–Parr nonlocal functional (LYP). The extent of the molecules in space was calculated for the energetically favorable conformation (geometrically optimized molecule) and their sizes and shapes were analyzed. The dimensions of molecules in three-dimensional space are measured according to the procedure detailed elsewhere [29]. The three largest dimensions ($a \times b \times c$) of propene (**1**), benzene (**2**), IPB (**3**), 1,2-DIPB (**4**), 1,3-DIPB (**5**), 1,4-DIPB (**6**), and 1,3,5-TIPB (**7**) molecules in mutually perpendicular directions are given in Table 1. The qualitatively structural fittings of the molecules inside the AFI ($AlPO_4$-5) molecular sieve were studied by MG as well as a comparison of the dimensions of the molecules with pore diameters. AFI lattice was generated from X-ray crystal reported by Bennett et al. [30]. Further, the chemical interaction between the zeolite host and guest molecules was studied using energy minimization calculations to understand the adsorption sites and diffusion characteristics of molecules **1**–**7**. The simulation box contained the zeolite generated from its crystal structure and the actual dimension of the simulation box is a $2 \times 2 \times 7$ unit cell (1.272 and 0.848 nm, a and b and c, respectively). The sizes of the simulation boxes are chosen in such a way that the symmetry along the channel direction is taken care of and the box is just large enough in the other two directions to take care of the nonbonded interactions, whose cutoff distance was taken as 0.95 nm. The diffusion energy profiles symmetrically repeat themselves in each unit cell, indicating the validity of the simulation box size, potential parameters, and energy minimization calculation procedures. The calculations were performed following the well-established forced diffusion procedure. This procedure has been widely used to study the diffusion of methanol, toluene nitration, isomers of butane, isomers of aromatic hydrocarbons, such as alkylnaphthalene, isobutylethylbenzene, and xylene, and isomers of acyl-2-methoxynaphthalene and acyl-4-hydroxyphenol [31,32]. Here, we investigated the diffusion of IPB and DIPB over $AlPO_4$-5. The sorbate molecule was forced to diffuse in regular steps of 0.02 nm along the diffusion path within the channel. At each point, a strong harmonic potential constrains the molecule to lie at a fixed distance from the initial position while the energetically favorable conformation and orientation of the molecules are derived by varying the internal degrees of freedom as well as nonbonding interaction of the molecule with the zeolite framework. The interaction energy at each point is calculated using

$$\text{interaction energy} = E_{\text{zeolite: molecule complex}} - (E_{\text{zeolite}} + E_{\text{molecule}}). \quad (1)$$

Thus, the diffusion energy profile is a graph showing the variation of interaction energy between a single molecule and the zeolite framework as the molecule diffuses within the channel of the zeolite. The diffusion energy profiles are useful to identify the most favorable (minimum energy) and unfavorable (maximum energy) adsorption sites for the molecules inside the zeolite channels. The difference in energy between the most favorable and most unfavorable sites in the diffusion energy profile gives the diffusion energy barrier for self-diffusivity. During these calculations of the interaction energy the atoms in the zeolite lattice are held fixed at their crystallographically determined geometries, whereas the guest molecules are flexible. Since our interest is to study the influence of the pore architecture and the dimensions on the diffusion characteristics of the molecules, we considered Al/P ratio 1/1 constant [30]. The influence of the presence of more molecules on the diffusivity (mutual effect) and the influence of temperature are not considered here. In view of these approximations, suitable care was taken to interpret the results.

3. Results and discussion

3.1. Characterization of MAPO-5 molecular sieves

3.1.1. Structures of MAPO-5 molecular sieves

All MAPO-5 in the present study was synthesized by the VPT method. Typical XRD patterns of calcined samples are shown in Fig. 1. The phase purity of the molecular sieves exhibited high crystallinity for all types of MAPO-5, and impure phases were not detectable. Their structures were stable after calcination at 550 °C for 7 h in dry air. Peak intensities slightly decreased in the order Mg > Ca > Sr > BaAPO-5. However, peak intensities of MgAPO-5 remained at a similar level for different MgO/Al_2O_3 ratios. Nitrogen adsorption measurements of calcined forms of Mg-free $AlPO_4$-5 and MgAPO-5 gave quite similar Type I isotherms, indicating that all molecular sieves have micropores. Micropore volumes are in the range of 0.111–0.122 ml/g, which are typical values for 12-ring one-dimensional channels [33]. This means that MAPO-5 molecular sieves have high phase purities, and any occluded material does not block their channels. Their surface areas are in the order of Mg > Ca > Sr > BaAPO-5.

Particles of MAPO-5 molecular sieves are observed as agglomerates of very small particles less than 1 μm as shown in Fig. 2. Crystal sizes were in the order Mg > Ca > Sr > BaAPO-5.

ICP analysis of as-synthesized MgAPO-5 shows that the MgO/Al_2O_3 ratio was higher in products than in starting gels (Table 2). These results suggest that a part of Al^{3+} was isomorphously substituted by Mg^{2+} in the framework.

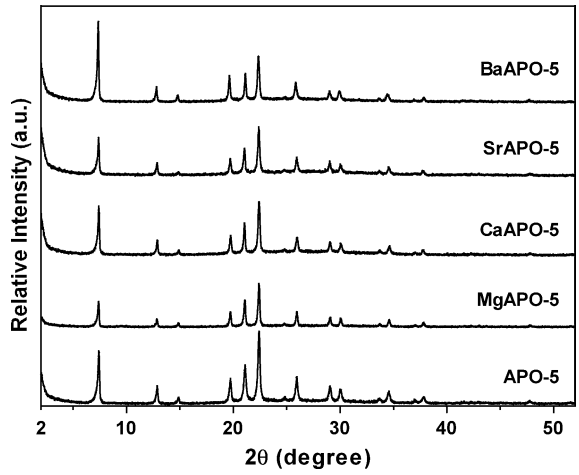

Fig. 1. XRD patterns of calcined samples of MAPO-5 and $AlPO_4$-5 molecular sieves.

A similar tendency was confirmed for Ca and SrAPO-5. However, BaAPO-5 gave the reverse results that values in products were lower than in starting gels. These results suggest that Ba^{2+} participates in framework by the substitution of Al^{3+}; however, there is a possibility that a part of Ba is not in the framework because Ba^{2+} is too large to substitute completely with Al^{3+}.

FT-IR spectra of pure $AlPO_4$-5 and MAPO-5 in the framework vibration range (800–1500 cm^{-1}) were recorded for calcined samples. Strong absorption by framework vibration was observed in the region of 1000–1250 cm^{-1}. Broad bands in the region of 1000–1100 cm^{-1} are characteristic of zeolitic materials, which are assigned to asymmetric stretching of tetrahedral Al–O and P–O [24]. Wavenumbers of MAPO-5 were higher than that of aluminosilicate; the presence of large amounts of phosphorous is responsible for this shift [34]. Pure $AlPO_4$-5 and MAPO-5 exhibited similar patterns of FT-IR spectra. However, the band shift toward higher frequencies was observed on alkaline earth metals in $AlPO_4$-5 substituted with Al^{3+} in the framework. The alkaline earth metals in the framework in the 12-membered ring lead to concomitant reduction in Al–O and P–O bond strength in the framework. The greater the charge transfer from O^{2-} to substituted alkaline earth metal cations (M–O bond increases from Mg to Ba), the weaker the (T–O) bond, and hence, observed bands shift to the higher frequencies [35]. Our results indicate that a strong vibration band around 1132 to 1135 cm^{-1} was shifted toward higher wave number; however, this shift is not so significant due to low concentrations of alkaline earth metal in the framework [26].

Unit cell parameters were calculated to confirm the isomorphous substitution of alkaline earth metals into the framework (Table 2) for all calcined samples. Because of the difference in T–O bond distance among Mg (1.85), Ca (2.17), Sr (2.36), Ba (2.54), Al (1.73), and P (1.54), an increase in cell volume is expected if Al or P is replaced by other metals [24,36]. If the variation observed in XRD could be taken as evidence that the metal was isomorphically

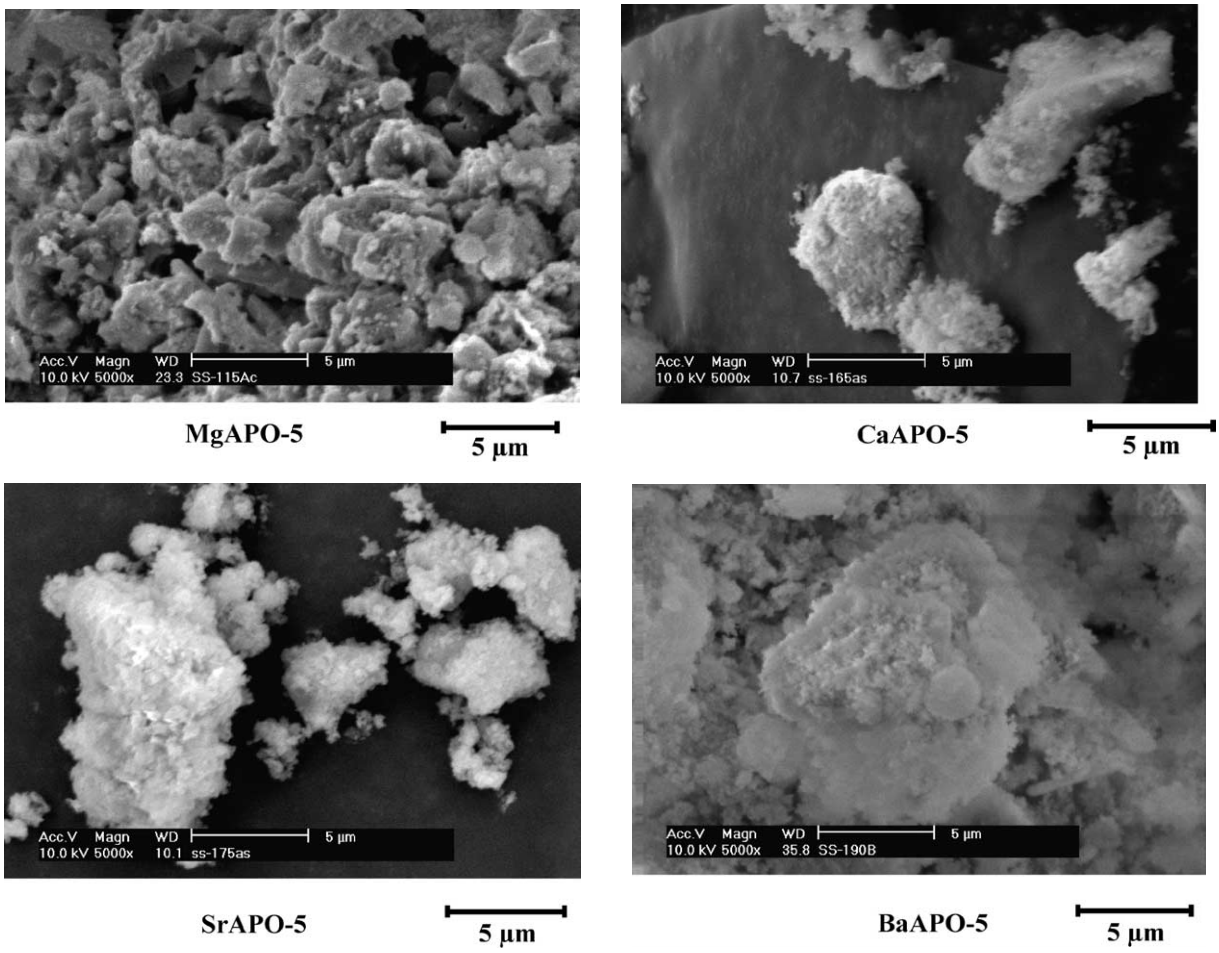

Fig. 2. SEM images of typical MAPO-5 molecular sieves.

Table 2
Physicochemical properties of MAPO-5 and $AlPO_4$-5 molecular sieves

M	Surface area (m^2/g)	MO/Al_2O_3		Unit cell parameters (Å)		
		Gel	MAPO-5[a]	$a = b$	c	V[b]
–	270.4	–	–	13.6630	8.4305	1362.96
Mg	282.7	0.025	0.027	13.7035	8.4687	1377.24
Mg	258.0	0.05	0.058	13.7093	8.4646	1377.75
Mg	271.1	0.10	0.128	13.7174	8.4644	1379.35
Ca	248.2	0.10	0.170	13.7133	8.4788	1380.86
Sr	205.6	0.10	0.174	13.7434	8.4701	1384.31
Ba[c]	172.3	0.10	0.083	13.7147	8.4735	1381.23

Gel composition: 1.0 Al_2O_3:0.1 MO:1.0 P_2O_5:0.76 Et_3N:45 H_2O (all samples crystallized at 175 °C except Ba).
[a] Determined by inductively coupled plasma atomic emission spectroscopy (ICP-AES).
[b] Unit cell volume.
[c] Crystallization temperature = 200 °C.

incorporated in the framework [36]. Hexagonal unit cell parameters, a and c, and cell volume are shown in Table 2. In the case of the variation of MAPO-5, unit cell parameters a and b and unit cell volume increases as a function of types of metal, whereas unit cell parameter c follows the opposite trend. $AlPO_4$-5 shows lower unit cell parameters a and c and unit cell volume as compared to MAPO-5. These results agree well with earlier work [36]. These unit cell parameters support strongly that alkaline earth metals were incorporated in the framework structure of 12-membered ring $AlPO_4$-5 structure.

3.1.2. Acidic properties of MAPO-5 molecular sieves

Temperature-programmed desorption of ammonia (NH_3-TPD) gives useful information on acid strength and amount of microporous materials. Fig. 3 shows typical NH_3-TPD profiles of MgAPO-5 with different MgO/Al_2O_3 ratios. Pure $AlPO_4$-5 showed a desorption peak (l peak) at about

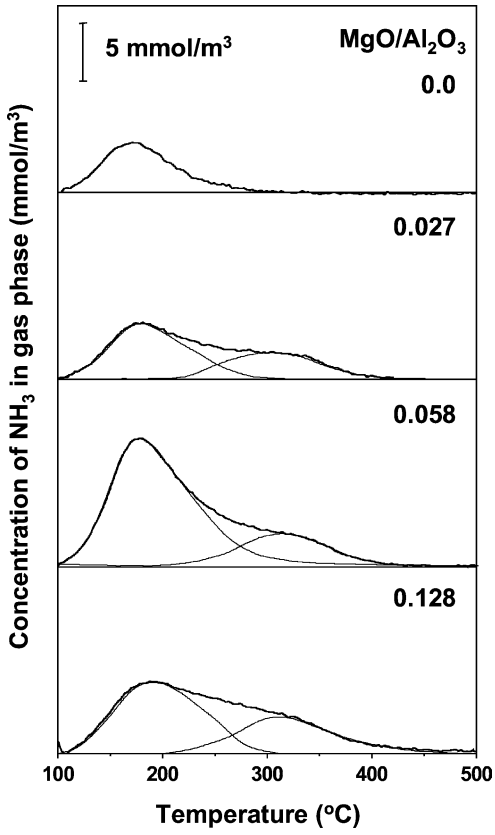

Fig. 3. NH_3-TPD profiles of MgAPO-5 molecular sieves with different MO/Al_2O_3 ratios.

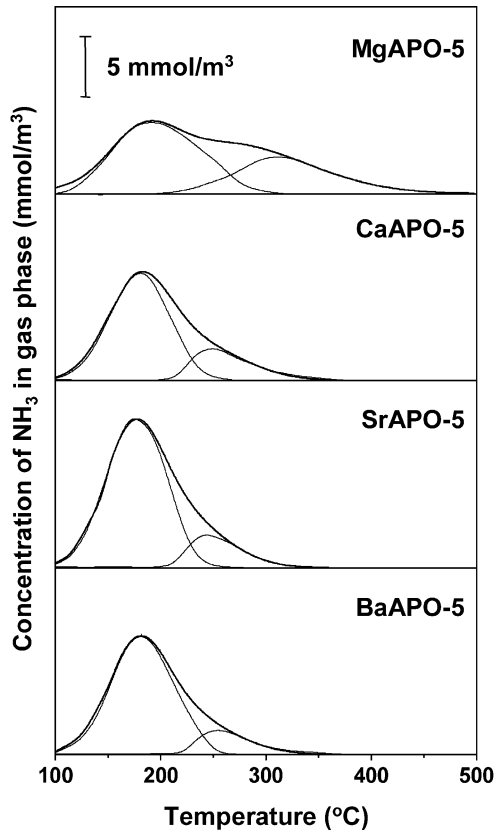

Fig. 4. NH_3-TPD profiles of MAPO-5 and $AlPO_4$-5 (M = Mg, Ca, Sr, and Ba). $MO/Al_2O_3 = 0.1$ (input ratio).

170 °C, which is due to physical adsorption of ammonia. However, MgAPO-5 had a desorption peak (*h* peak) around 250–350 °C. This peak is due to the acidity of MgAPO-5 by isomorphous substitution of Mg^{2+} with Al^{3+}. Fig. 4 shows NH_3-TPD profiles of MAPO-5 with $MO/Al_2O_3 = 0.10$ (input ratio). A small *h*-peak was observed for Ca, Sr, and BaAPO-5 except MgAPO-5. These results show that MgAPO-5 has the strongest acidity with the largest amounts, and that Ca, Sr, and BaAPO-5 also have acidity in smaller amounts, although they are weaker than MgAPO-5.

FT-IR spectra of pyridine adsorbed on MAPO-5 ($MO/Al_2O_3 = 0.1$) synthesized by the VPT method were recorded. MgAPO-5 exhibited several peaks due to pyridinium ions on Brønsted acid sites (B: 1546 and 1641 cm^{-1}) and Lewis bounded pyridine (L: 1456 and 1618 cm^{-1}). A peak at 1492 cm^{-1} can be assigned to pyridine associated with both Brønsted and Lewis acid sites. The intensities of these peaks increased with the amounts of Mg: this is consistent with NH_3-TPD spectra (results are not given). The effects of types of alkaline metal on the IR-spectra of pyridine adsorbed show that peak intensities were weak for Ca, Sr, and BaAPO-5: this corroborates with NH_3-TPD spectra. The results by NH_3-TPD and pyridine adsorption indicate that the acidity of MAPO-5 decreases in the order Mg ≫ Ca > Sr > BaAPO-5 (results not shown) [38].

The catalytic activities of the cracking of IPB and 1,3,5-TIPB over MAPO-5 and $AlPO_4$-5 are examined to elucidate the activity of external acid sites. Typical results are shown in Table 3. The catalytic activity for the cracking of IPB over MAPO-5 was in the order Mg ≫ Ca > Sr > BaAPO-5 > $AlPO_4$-5. The catalytic activity of cracking of 1,3,5-TIPB was much less over MAPO-5 and AlPO-5 as compared to cracking of IPB: 1,3,5-TIPB cannot enter into the pore of $AlPO_4$-5. These results suggest that external surface acidity also decreased as the acidity of the MAPO-5 decreased.

Table 3
Cracking of IPB and 1,3,5-TIPB over MAPO-5[a] and $AlPO_4$-5 molecular sieves

MAPO-5	Conversion (%)	
	IPB	1,3,5-TIPB
–	2.5	2.0
Mg	98.7	8.2
Ca	20.2	4.3
Sr	5.3	3.5
Ba	2.9	3.2

[a] $MO/Al_2O_3 = 0.1$ (input ratio).

3.2. Catalytic isopropylation of benzene over MAPO-5 molecular sieves

3.2.1. Influence of types of alkaline earth metal

Fig. 5 shows the influences of type of alkaline earth metals in MAPO-5 ($MO/Al_2O_3 = 0.1$ (input ratio)) for the

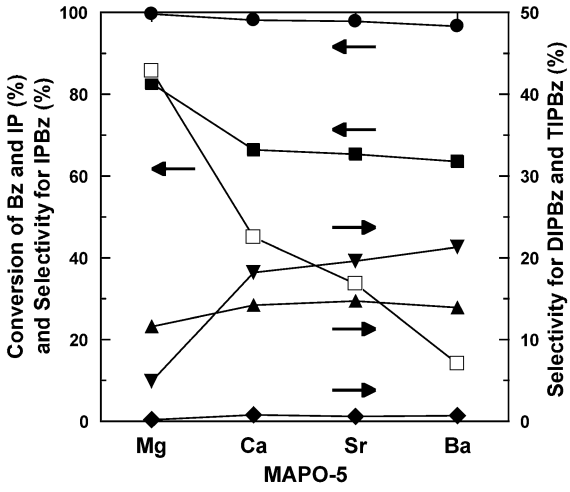

Fig. 5. Influence of metal type of MAPO-5 on conversion and product selectivity in the isopropylation of benzene with 2-propanol. Reaction conditions: temperature = 275 °C; TOS = 6 h; feed: B/IP = 6; MO/Al_2O_3 = 0.1 (input ratio); WHSV = 3.5 h^{-1}. Legends: conversion: □, benzene; ●, 2-propanol; selectivity: ■, IPB; ▼, 1,4-DIPB; ▲, 1,3-DIPB; ◆, 1,3,5-TIPB.

isopropylation of benzene with 2-propanol. Catalytic activity was in the order Mg ≫ Ca > Sr > BaAPO-5 > $AlPO_4$-5. The decrease in the selectivity of IPB was observed with increase in DIPBs from Mg to BaAPO-5. The selectivity of IPB decreased with acidity of the catalyst in the order Mg ≫ Ca > Sr > BaAPO-5, and an increase in the selectivity of DIPBs was observed simultaneously in that order. This is the expected order from acidic character. However, no higher aromatics were detected in the product. Selectivity of TIPB was observed less than 0.5%. Sasidharan et al. reported similar changes of the selectivity of IPB and DIPB in the isopropylation of benzene over NCL-1 zeolite: a decrease of the selectivity of IPB and an increase in the selectivity of DIPB were accompanied by an increase of SiO_2/Al_2O_3 ratio [18].

The isopropylation of benzene with 2-propanol is multistep and sequential reaction. The main reaction can be represented as follows:

$$\text{IP} \rightarrow \text{propene} + \text{water}, \quad (1)$$

$$\text{B} + \text{propene} \rightarrow \text{IPB}, \quad (2)$$

$$\text{IPB} + \text{propene} \rightarrow \text{DIPB} \quad (\text{the isomerization of 1,2- or 1,4-DIPBs to 1,3-DIPB}), \quad (3)$$

$$\text{DIPB} + \text{B} \rightarrow 2\text{IPB}, \quad (4)$$

$$\text{DIPB} + \text{propene} \rightarrow \text{TIPB}, \quad (5)$$

$$\text{TIPB} + \text{B} \rightarrow 2\text{DIPB}, \quad (6)$$

$$2\text{IPB} \rightarrow \text{DIPB} + \text{B}. \quad (7)$$

The low selectivity of IPB over less acidic catalysts is considered for the following reasons:

(i) Propene is obtained in reaction products in trace amounts (reaction (1)). Alkylation of IPB (reaction (3)) is faster than alkylation of benzene (reaction (2)) [37] because of the acceleration by the electron-donating nature of the isopropyl group.

(ii) Transalkylation of DIPB with benzene (reaction (4)) and cracking of DIPB (reaction (3) reverse) requires strong acid sites [8,18]. Alkylation of benzene with 2-propanol or propene is an acid-catalyzed reaction, which readily takes place on Brønsted acid sites on zeolites [5].

(iii) It is also possible that cracking of IPB (reaction (2) reverse and reaction (7)) [12,13,25] to benzene and propene may also contribute to decrease the selectivity of IPB. Corma et al. [21] have already reported that very small amounts of acid sites are needed for IPB cracking.

The conversion of benzene (theoretical maximum conversion based on B/IP ratio) relates directly to the acid strength of the catalyst as discussed above. However, the overall conversion of 2-propanol to propene remains constant ∼ 99 ± 1% for all MAPO-5. These results suggest that the isopropylation of benzene and the dehydration of 2-propanol have different characters of active sites on MAPO-5. The similar types of observation were reported by Sasidharan et al. over large-pore NCL-1 zeolites [18], Das et al. over sulfated ZrO_2–TiO_2 for the isopropylation of benzene [20], and Reddy et al. for the isopropylation of toluene over H-BEA zeolites [16b].

Among the DIPB isomers, the decrease of the selectivity of 1,3-DIPB accompanied an increase in the selectivity of 1,4-DIPB: this is also due to the decreasing of acidity of MAPO-5 (Fig. 5). 1,3-DIPB was predominant over 1,4-DIPB in the case of MgAPO-5, whereas a reverse trend was observed over Ca, Sr and BaAPO-5 and pure $AlPO_4$-5 catalysts.

TIPB may be formed by the alkylation of 1,3-DIPB with propene (reaction (5)). It can further disproportionate with benzene and form DIPB (reaction (6)). The ratio of 1,4-/1,3-DIPB increased from Mg to BaAPO-5. These results indicate that the isomerization of 1,3-DIPB was less favorable over weak acid catalysts such as Sr and BaAPO-5.

The selectivity of IPB decreased from Mg to BaAPO-5 by accompanying the increase of DIPBs (Fig. 5). The total selectivity of IPB and DIPBs for MAPO-5 catalysts remained almost constant at about ∼ 97 ± 2%, and the selectivity of TIPB is ∼ 1 ± 0.5%.

The alkylation of benzene over acidic catalyst is an electrophilic reaction. Hence, among DIPBs, 1,2- and 1,4-DIPBs can be formed as a primary product preferentially via the isopropylation of IPB. However, in the present study, 1,2-DIPB was formed only in trace amounts (less than 0.2%), and 1,3- and 1,4-DIPBs was more predominant in accordance with earlier studies of the zeolite and metal oxides [4–17]. It is clear that the formation of 1,2-DIPB is less favorable due the steric hindrance of the isopropyl group on IPB. Experiments also confirmed that the steric hindrance is more predomi-

nant for the formation of 1,2-DIPB because no traces of 1,2-DIPB isomer were observed even in beta zeolite, MCM-41, and metal oxide [4,5,7,19,20]. This conclusion is further supported by a molecular modeling study; the total energy observed for full geometrically optimized molecules of 1,2-, 1,3-, and 1,4-DIPBs are given in Table 1. From these results, it is clear that 1,3-DIPB is more thermodynamically stable than other isomers. The band gap of the highest occupied molecular orbital (HOMO) and the lowest occupied molecular orbital (LUMO) decreases from 1,2- to 1,4-DIPB isomer. The formation of *ortho*- and *para*-substituted products should be more plausible than the *meta*-substituted because the alkylation is an electrophilic reaction. However, 1,3-DIPB was more predominant than 1,4-DIPB over MgAPO-5 catalysts. This is due to either via the isomerization of 1,4-DIPB to 1,3-DIPB (reaction (3)) or via the disproportionation of IPB to benzene and DIPB (reaction (7)). In the case of Ca, Sr, and BaAPO-5, the isomerization may not be possible, and 1,4-DIPB was more predominant than 1,3-DIPB over these catalysts. This may be due to lower acidity of Ca, Sr, and BaAPO-5 catalysts.

3.2.2. Isopropylation of benzene over MgAPO-5 molecular sieves

MgAPO-5 molecular sieves have the highest catalytic performance for the isopropylation of benzene among MAPO-5 as discussed above. Hereafter, the parameters, such as MgO/Al_2O_3 ratio, reaction temperature, WHSV, B/IP ratio of feed, and TOS are discussed to elucidate the solid acid catalysis over MgAPO-5 molecular sieves.

3.2.2.1. Influence of MgO/Al_2O_3 ratio. The influence of MgO/Al_2O_3 ratio for MgAPO-5 was studied at 275 °C, TOS = 6 h, and B/IP = 6 (molar ratio). The typical results are shown in Table 4. Conversion of benzene increased with the ratio and reached a maximum at 0.01. However, the conversion of benzene for $AlPO_4$-5 was 10-fold less compared to MgAPO-5. Catalytic activity is correlated with the acidity of the molecular sieves. Conversion of 2-propanol was ∼ 100% for all samples (MgO/Al_2O_3 = 0.025, 0.05, and 0.1) except $AlPO_4$-5 as shown in Table 4.

The selectivity of IPB for the MgO/Al_2O_3 ratio decreased in the order 0.1 > 0.05 > 0.025 > 0.0, whereas DIPBs followed in the reverse order. The selectivity of TIPB observed is less than 0.5% for MgAPO-5 and $AlPO_4$-5.

The selectivity for 1,3-DIPB was always higher than 1,4-DIPB for all MgO/Al_2O_3 ratios. However, this trend was reversed in the case of pure $AlPO_4$-5. Even though the total selectivity for IPB and DIPBs was noted as 98 ± 1%. It is also observed that the 1,4-/1,3-DIPB ratio is less (0.38) for MgO/Al_2O_3 = 0.05 and was higher for 0.025 and 0.1.

3.2.2.2. Influence of reaction temperature. Temperature has a paramount effect in the product distribution for the isopropylation of benzene as shown in Fig. 6. Conversion of benzene and the selectivity of IPB increased with reaction temperature; however, the selectivities of DIPBs and TIPB were decreased. These results could be due to the transalkylation of DIPBs and TIPBs to IPB [18]. The formation of TIPB (> 0.5%) was observed in the product at lower temperatures (below 225 °C). TIPB may also be favorable at higher temperatures (above 225 °C); however, it was observed only in a small amount: much of them may transalkylate with benzene (reaction (6)) to DIPB. 1, 4-DIPB was predominant than 1,3-DIPB at lower temperatures; however 1,3-DIPB was predominant over 1,4-DIPB at higher temperatures. These changes may be due to the fact that the alkylation of IPB (reaction (3)) competes favorably with transalkylation of DIPB with benzene to IPB (reaction (4)).

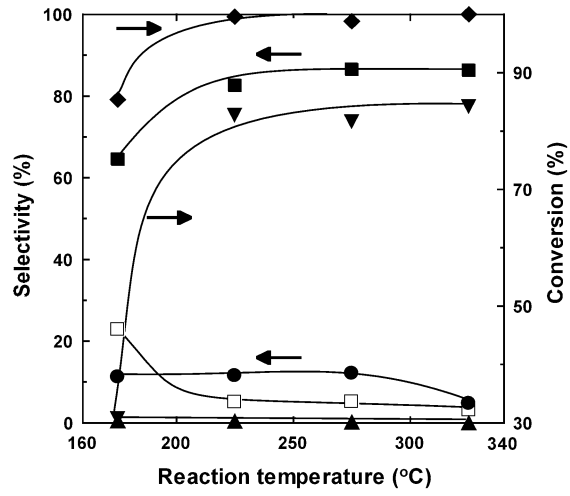

Fig. 6. Influence of temperature on conversion and product selectivity in the isopropylation of benzene over MgAPO-5 catalyst. Reaction conditions: TOS = 6 h; feed: B/IP = 6; MgO/Al_2O_3 = 0.1 (input ratio); WHSV = 3.5 h^{-1}. Legends: conversion: ▼, benzene; ◆, 2-propanol; selectivity: ■, IPB; □, 1,4-DIPB; ●, 1,3-DIPB; ▲, 1,3,5-TIPB.

Table 4
Influence of MgO/Al_2O_3 ratio on conversion of benzene and selectivity of products in the isopropylation of benzene to 2-propanol

MgO/Al_2O_3	Conversion (%)	Selectivity (%)					
		IPB	1,2-DIPB	1,3-DIPB	1,4-DIPB	1,3,5-TIPB	Others[a]
0.0	8.4	52.0	0.0	15.9	31.9	0.0	0.2
0.025	80.1	80.5	0.2	13.1	5.6	0.5	0.1
0.05	86.6	82.1	0.2	10.1	6.9	0.5	0.2
0.10	85.7	82.8	0.2	11.5	5.0	0.2	0.3

[a] Others includes C_6–C_8 aromatics, propylbenzene, toluene. Reaction conditions: temperature = 275 °C; TOS = 6 h; WHSV = 3.5 h^{-1}; feed, B/IP = 6.

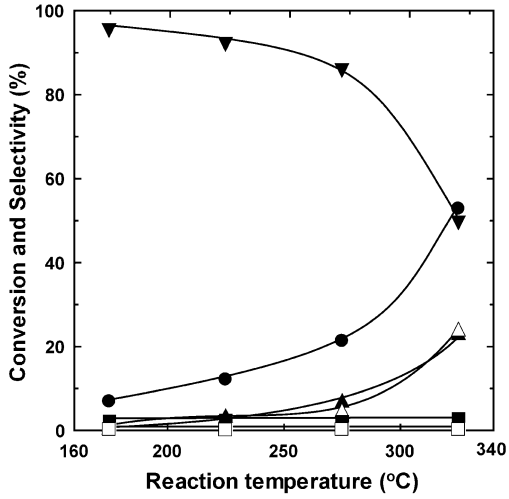

Fig. 7. Influence of the temperature on product selectivity in the isomerization of 1,4-DIPB over MgAPO-5. Reaction conditions: TOS = 2 h; feed: 1,4-DIPB/IP = 6; MgO/Al_2O_3 = 0.1 (input ratio); WHSV = 3.5 h^{-1}. Legends: ●, conversion of 1,4-DIPB; selectivity: ▲, IPB; ▼, 1,4-DIPB; △, 1,3-DIPB; □, others; ■, benzene.

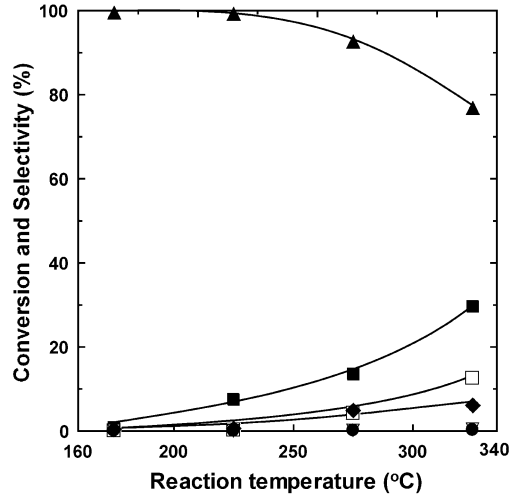

Fig. 8. Influence of the temperature on product selectivity in the isomerization of 1,3-DIPB over MgAPO-5. Reaction conditions: TOS = 2 h; feed: 1,3-DIPB/IP = 6; MgO/Al_2O_3 = 0.1 (input ratio); WHSV = 3.5 h^{-1}. Legends: ■, conversion of 1,3-DIPB; selectivity: □, IPB; ◆, 1,4-DIPB; ▲, 1,3-DIPB; ▽, others; ●, benzene.

However, transalkylation (reaction (4)) may be more predominant, and eventually an increase in the selectivity of IPB was observed. The total selectivity for IPB and DIPBs is ∼ 97 ± 2% above 225 °C. Thermodynamically stable 1,3-DIPB is more favorable than 1,2- and 1,4-DIPB isomers at temperatures above 225 °C. It is also observed that 1,4-DIPB isomerizes to 1,3-DIPB isomer above 225 °C (shown in Fig. 7). These results are in agreement with DFT calculations. Fully optimized organic molecules by DFT at the B3LYP level of theory using the 6-311G (d,p) basis set revels that 1,3-DIPB is more stable than 1,2- and 1,4-DIPB isomers (Table 1). Similar types of observations are reported in earlier literature over NCL-1 and ZrO_2–TiO_2 by Sasidharan et al. [18] and Das et al., respectively [20]. In fact, Siffert et al. [12] considered the catalyst characteristics, i.e., the interaction of silanols present on H-BEA zeolite surface with the reactant and product molecules, which increases the diffusion barriers for DIPBs. Taking this into consideration, they could explain this by the lower apparent activation energy for the isopropylation of benzene reported in the literature [12]. Interestingly, the selectivity of 1,3-DIPB above 275 °C in our case slightly decreased with subsequent increase in 1,4-DIPB selectivity, probably due to the thermodynamic effect observed by Valtierra et al. [5]. Based on these observations we can conclude that the stability of 1,3-DIPB is determined by the catalyst characteristics up to 275 °C, and the catalysis is a thermodynamically controlled process above 275 °C [20]. IPB was increased initially, but then became steady, whereas DIPB decreased with temperature. The selectivity of TIPB is less than 0.5%.

The isomerization of 1,4- and 1,3-DIPBs was carried out over MgAPO-5 at WHSV 3.5 h^{-1} and TOS 2 h, and the results are shown in Figs. 7 and 8. The conversion increased with the temperature, and the conversion of 1,4-DIPB was higher than that of 1,3-DIPB. The selectivity of IPB also increased with temperature, and accompanied the decrease in the selectivity of benzene for the isomerization of 1,4-DIPB. Although a similar trend was observed in the isomerization of 1,3-DIPB, the selectivity of IPB was less compared to the isomerization of 1,4-DIPB in Fig. 7. These results indicate that dealkylation of IPB occurs at low temperature to form benzene (below 175 °C). However, dealkylation of DIPB as well as alkylation of IPB was observed at higher temperatures. The dealkylation rate is less for 1,3-DIPB compared to 1,4-DIPB. The probable reason for the selectivity of IPB in the DIPB isomerization are (i) Dealkylation of DIPB takes place even at lower temperatures to form benzene (reaction (2) reverse); this reaction retards at higher temperatures. (ii) DIPB is dealkylated to form IPB as a major product at higher temperatures (reaction (3) reverse). (iii) It is also possible that 1,4-DIPB is isomerized to thermodynamically stable product 1,3-DIPB (reaction (3)). In the isomerization of 1,4- and 1,3-DIPBs, TIPB was observed in a small amount. It indicates that DIPB was dealkylated to form propene and IPB, and that propene again alkylated DIPB to form TIPB as by-product (reaction (5)).

3.2.2.3. Influence of benzene: 2-propanol molar ratio. The influence of B/IP molar ratio of feed on conversion and product distribution is shown in Table 5. For all the ratios of feed studied, conversion of IP remained at ∼ 98 ± 1 mol%, but conversion of benzene decreased with increase in B/IP ratio. As expected, the selectivity of IPB increased with the increase in B/IP molar ratio, and accompanied the decrease in the selectivity of DIPB. At the same time, the total selectivity of IPB and DIPBs remained constant. IP and propene were also detected at low B/IP molar ratios. The selectivity for higher alkylated and cracking/disproportionation products decreased with the increase in the ratio. The decreases in the selectivity for DIPB and TIPB are due to the fact that

Table 5
Effect of feed molar ratios in the isopropylation of benzene to 2-propanol over MgAPO-5 catalysts

B/IP ratio	Conversion (%)	Selectivity (%)					
		IPB	1,2-DIPB	1,3-DIPB	1,4-DIPB	1,3,5-TIPB	Others[a]
3	81.8	59.8	0.6	28.0	11.3	0.3	0
6	85.7	82.8	0.2	11.5	5	0.2	0.3
9	76.7	83.5	0.1	10.7	5.1	0.3	0.3
12	64.7	83.2	0.1	10.6	5.6	0.3	0.2

Reaction conditions: $Mg/Al_2O_3 = 0.1$ (input ratio); temperature = 275 °C; WHSV = 3.5 h^{-1}; TOS = 6 h.
[a] Others includes C_6–C_8 aromatics, propylbenzene, toluene.

Table 6
Influence of weight hourly space velocity (WHSV) on conversion of benzene and selectivity of products in the isopropylation of benzene with 2-propanol over MgAPO-5 catalysts

WHSV (h^{-1})	Conversion (%)	Selectivity (%)					
		IPB	1,2-DIPB	1,3-DIPB	1,4-DIPB	1,3,5-TIPB	Others[a]
2.0	86.9	85.1	0.2	10.7	4.0	0.0	0.0
3.5	85.7	82.8	0.2	11.5	5.0	0.2	0.3
5.0	68.4	69.0	0.1	18.6	11.8	0.3	0.2
7.0	34.8	68.1	0.1	18.5	12.8	0.3	0.2

Reaction conditions: $Mg/Al_2O_3 = 0.1$ (input ratio); temperature = 275 °C; TOS = 6 h; feed, B/IP = 6.
[a] Others includes C_6–C_8 aromatics, propylbenzene, toluene.

transalkylation of these products was more favored with the increase of B/IP ratio. Less than 0.2% of TIPB was obtained at the ratio of 6, and the decrease of DIPB was observed with the increase of the selectivity of IPB by the increase of molar ratio to 12. For all cases, the total selectivity of IPB and DIPBs was varied between 98 and 99%. From these results, the B/IP ratio was required to be at least 6 to achieve selectivity of 100% toward isopropyl derivatives of benzene under these reaction conditions. In an earlier work, Siffert et al. [12] reported that propene is more strongly adsorbed than benzene on a beta zeolite surface. Therefore, the benzene to propene ratio increases the possibility of interaction of benzene with the catalyst surface resulting higher selectivity of alkylated product.

3.2.2.4. Influence of WHSV. The effect of WHSV on the product distribution is shown in Table 6. The conversion of benzene and the selectivity of IPB decreased with increasing WHSV. However, the selectivity of DIPBs increased with the increase of WHSV, and the total selectivity of IPB and DIPBs remained almost constant at about 97 ± 2%. The transalkylation (reaction (4)) enhances IPB as principal product at higher contact times (lower WHSV). 1,3-DIPB is predominant among the DIPBs at lower WHSV, but continuously decreased with the increase of 1,4-DIPB. The 1,3-/1,4-DIPB ratio decreased with the increase of WHSV: this may be due to less contact time. The selectivity of IPB decreased with the increase in DIPBs, whereas TIPB was observed less that 0.5%. However, conversion of 2-propanol was almost unchanged ∼ 98 ± 1% under all conditions.

3.2.2.5. Time on stream (TOS). Fig. 9 shows the effects of time on stream on catalytic activity and product distribution studied at 275 °C over MgAPO-5 for 12 h. The conversion of benzene decreased with time, initially a little faster and then became steady. However, conversion of IP remained ∼ 100%, which is mainly accounted for by the activity of the dehydration. Small amount of acid sites is enough for the dehydrogenation of 2-propanol to propene. After 12 h, the alkylation sites were slightly deactivated/poisoned (indicated by decrease in benzene conversion), but the dehydration of 2-propanol to propene is not affected as shown in Fig. 9. These results show that active sites for the dehydration of 2-propanol are active after long TOS. The increase

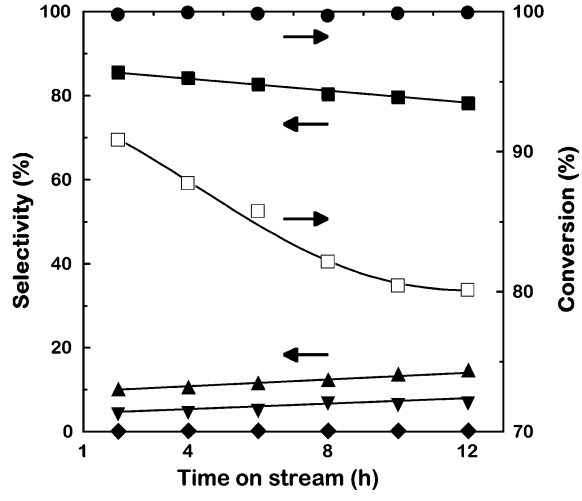

Fig. 9. Effect of time on stream on conversion and selectivities of products in the isopropylation of benzene with 2-propanol over MgAPO-5. Reaction conditions: 275 °C; feed: B/IP = 6; $MgO/Al_2O_3 = 0.1$ (input ratio); WHSV = 3.5 h^{-1}. Legends: conversion: □, benzene; ●, 2-propanol; selectivity: ■, IPB; ▼, 1,4-DIPB; ▲, 1,3-DIPB; ◆, TIPB.

of the selectivity of IPB accompanied the decrease of the selectivity of DIPBs with time on stream. Initially, the selectivity of IPB decreased faster up to 8 h and then became more or less steady. It is interesting to note that 1,3-DIPB is always predominant over 1,4-DIPB. The selectivity for 1,3-DIPB decreased with TOS accompanying the increase of 1,4-DIPB; this may be due to the deactivation of active sites. Total coke deposition 1.2% was detected after the duration of 12 h reaction over MgAPO-5 (reaction carried out at 275 °C). MgAPO-5 has straight 12-membered channels with mild acidity and without any side pockets. Most of the reports earlier have proposed that catalyst deactivation during the alkylation is due to coke deposition on the active sites [6,9]. Some reports have also been published correlating coke deposition and catalyst deactivation with acidic, textural, structural, and other parameters [13–15]. Pradhan and Rao reported that coke deposition for the isopropylation of benzene using propene over faujasite and mordenite zeolite were 14 and 7.5%, respectively [16]. In the present case, TOS studies at 225 °C indicate that more amounts of DIPB and TIPB were formed at the beginning of the reaction and decreased with TOS. This could be due to the more favored *trans*-alkylation of these derivatives initially, and then decreased with TOS. The selectivity of IPB decreased with TOS with a simultaneous increase of DIPB, whereas TIPB was not affected significantly.

3.3. Molecular modeling of the isopropylation of benzene over MAPO-5 molecular sieves

In order to clarify the influence of bulkiness of molecules on $AlPO_4$-5 pore diameter, we have selected all possible isomers formed in the isopropylation of benzene, viz. IPB, 1,2-, 1,3-, and 1,4-DIPBs and 1,3,5-TIPB. $AlPO_4$-5 has 12-membered straight channels having a diameter of 0.73 nm. The shape selectivity achieved by zeolites in catalytic conversion is governed by several factors, including pore diameters of the zeolites as well as the size and the shape of the molecules; the relative rates of diffusion of the reactants, products, and intermediate play dominant roles. Information about the interactions at the molecular level is difficult to derive experimentally. However, the diffusion energy profiles calculated from the interaction energies can predict the interactions, which are useful for deriving the diffusion barrier, and which provide a good indication of the relative rates of diffusion through the pores of molecular sieves. With recent advances in molecular graphics techniques, it is possible to derive accurately the shape and the size of the molecules. When we compare the dimensions of the molecules with the pore diameters of the molecular sieves, the largest dimension (longest dimension) (a) of the molecules will not play any significant role in shape selectivity. The molecules are known to take the orientation in which the largest dimension of the molecule lies along the length of the channel. In the specific case of isomers of DIPB, the smallest dimension of the molecule (the size of the isopropyl group) is the same for all the isomers. Thus, the second largest dimension of these isomers plays a crucial role. Based on these results, it is expected that zeolites with a pore diameter of 0.55 to 0.60 nm should be able to sieve **3** and **6** from **4** and **5**. The MG picture shows (Fig. 10) the fitting of **4**–**7** (IPB has the same dimensions; Table 1 in the b and c direction) (CPK model) inside $AlPO_4$-5 pores (cross section of 12-MR). The diffusion of **3**–**6** is possible, but diffusion of

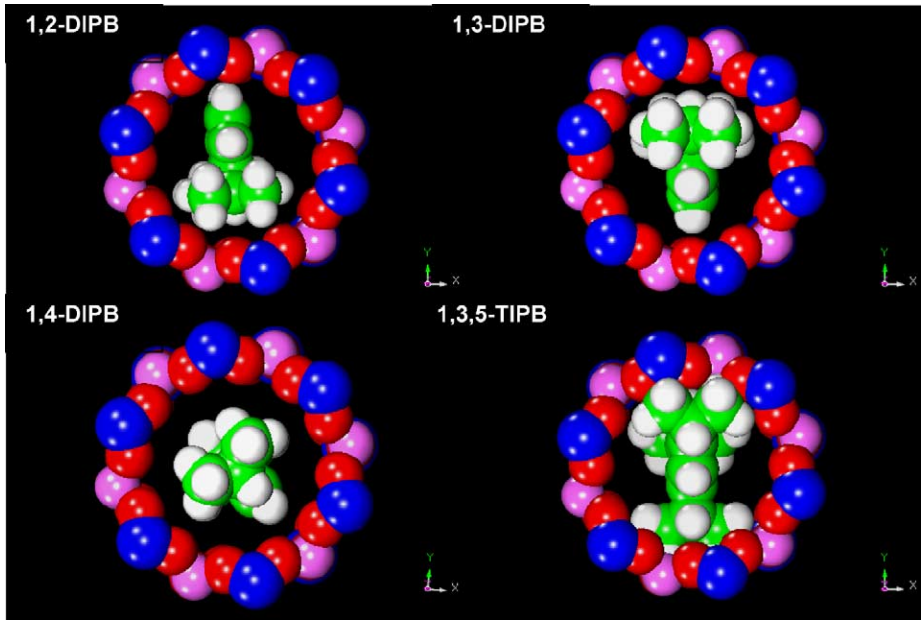

Fig. 10. MG picture shows the fitting of 4–7 (CPK model) inside $AlPO_4$-5 molecular sieves pores (cross section of the 12-MR). Hydrogen atoms are whitish gray, carbon atoms are green, phosphorous atoms are dark blue, oxygen atoms are red, and aluminum atoms are pink. Molecules **3**–**6** are very free fits, whereas **7** very tight fits in the pores of AFI (12-MR).

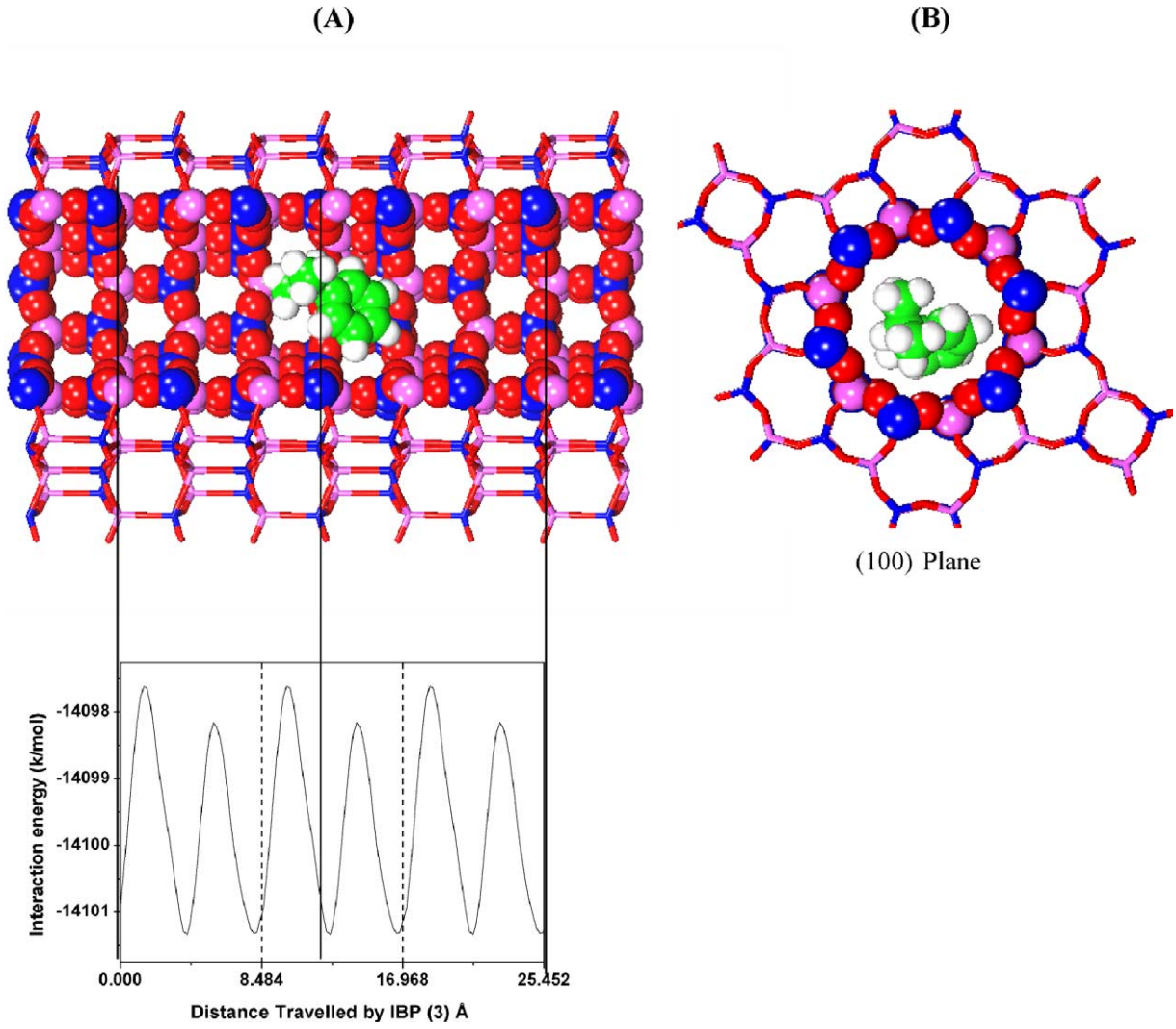

Fig. 11. (A) Variation of the interaction energy of **3** in the $AlPO_4$-5 framework as the molecule diffuses through the 12-M channel. The cross section of the 12-MR windows in the perpendicular direction is shown. (B) The 12-MR channel along the diffusion path. A typical minimum energy configuration of the molecule during the diffusion is shown.

7 is not possible. The diffusion of the molecules **1**–**7** along the *c* direction in the 12-MR straight channel was carried out. The molecules pass several minima and maxima, while diffusing through a unit cell. It is observed that molecules **3**–**6** have diffusion barriers in the same level. The diffusion barriers are in the order **4** > **5** > **3** > **6** (Table 1). The typical diffusion energy profiles for IPB and 1,4-DIPB are shown in Figs. 11 and 12, respectively. The diffusion barrier of IPB shows two minima, one at the center of the unit cell and another at the end of the unit cell. However, IPB shows two maxima, one at the 1/4 and another at 3/4 of the unit cell. The diffusion energy pattern of **7** shows that it cannot diffuse through the 12-MR of AFI. Similar results are observed experimentally in the cracking of 1,3,5-TIPB. Molecular modeling studies show that there is no shape selectivity for IPB formation. $AlPO_4$-5 molecular sieves can sieve on 1,3,5-TIPB.

4. Conclusions

AFI aluminophosphate molecular sieves partly substituted with alkaline earth metals in the framework (MAPO-5) exhibit high activity and selectivity in the isopropylation of benzene with 2-propanol to form IPB. The selectivity of IPB ranges between 85 to 95% over MAPO-5, and the total selectivity of IPB and DIPB is always over 95%. The highest conversion (96.6%) was achieved for MgAPO-5, and the lowest conversion (14.1%) was for BaAPO-5. These results suggest that MAPO-5 molecular sieves are catalytically active, and that catalytic activity decreases from Mg to Ba. Mild acidity is observed for Ca, Sr, and BaAPO-5 judging from NH_3-TPD, and cracking of 1,3,5-TIPB. They have enough acid strength for the alkylation of aromatic hydrocarbons, although catalytic activity depends on isomorphous substitution of alkaline earth metal. Selectivity of IPB deceases

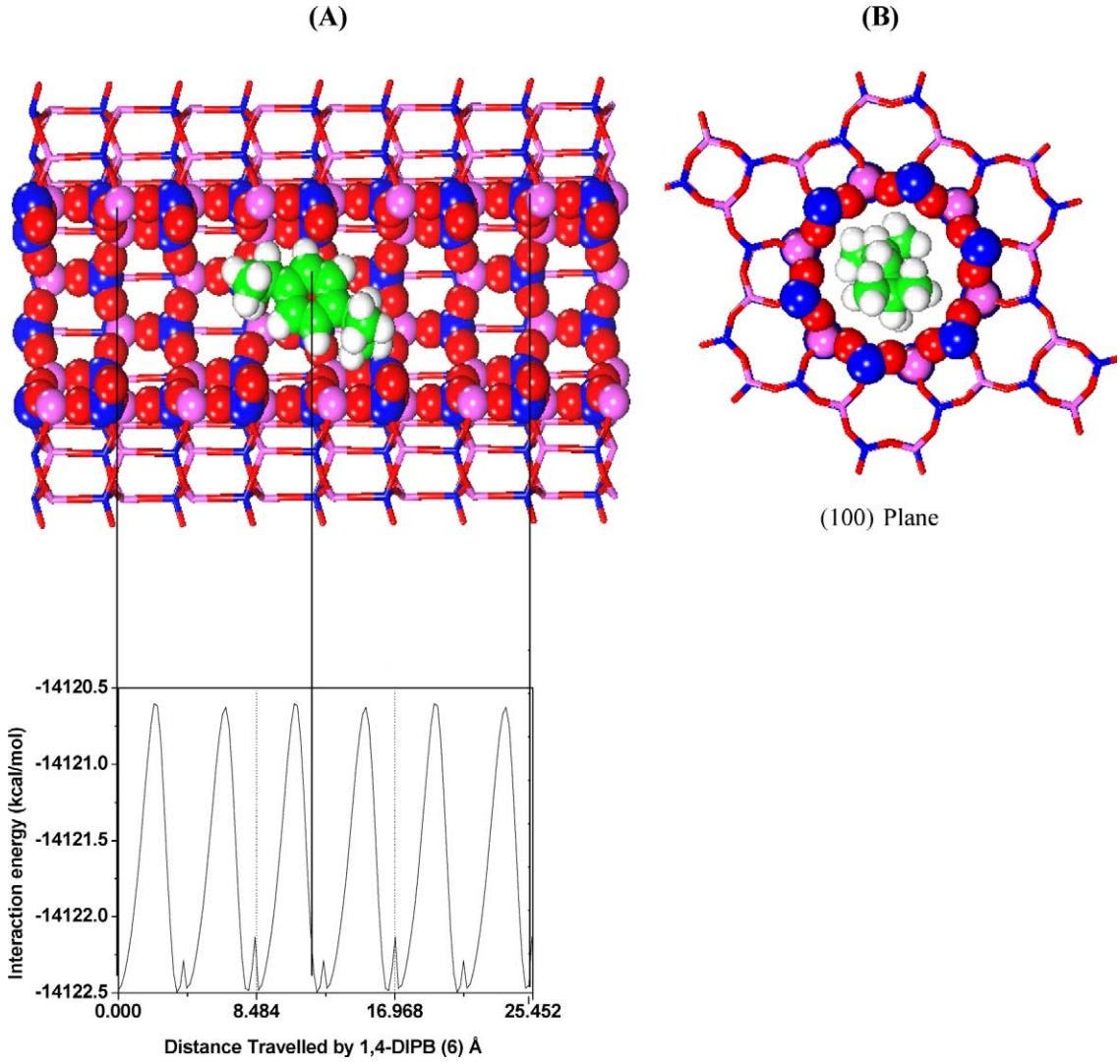

Fig. 12. (A) Variation of the interaction energy of **6** in the $AlPO_4$-5 framework as the molecule diffuses through the 12-MR channel. The cross section of the 12-MR windows in the perpendicular direction for the AFI framework is shown. (B) The 12-MR channel along the diffusion path. A typical minimum energy configuration of the molecule during the diffusion is shown.

with acidity of MAPO-5 and follows the above order. Conversion of 2-propanol is above $98 \pm 1\%$ for all the cases. With TOS, the alkylation sites were deactivated faster than the dehydration sites. Thermodynamically stable 1,3-DIPB is more favorable than 1,2- and 1,4-DIPB isomers at temperatures above 225 °C. In all cases, IPB was found as the major product, and DIPBs and TIPB as minor products. Among the DIPBs, 1,3-DIPB is predominating over 1,4-DIPB on more acidic catalyst and at higher temperatures. Propylbenzene was not detected in significant quantity in the product. Coke deposition of 1.2% is observed over MgAPO-5 catalyst. The isomerization of DIPB proceeds with dealkylation as well as alkylation of IPB and disproportionation to IPB and benzene.

Molecular modeling study shows that 1,3-DIPB is the most stable and bulkier among the DIPB isomers. Diffusional study shows that IPB and DIPBs are not shape-selectively formed in $AlPO_4$-5 pores. However, diffusion of 1,3,5-TIPB is difficult through 12-MR pores of $AlPO_4$-5 molecular sieves.

Acknowledgments

S.B.W. thanks the Japan Society for the Promotion of Science (JSPS) for a fellowship and S.K.S. is grateful to the Ministry of Education, Culture, Sports, Science, and Technology for the grant of a Japanese Government Scholarship.

References

[1] T.C. Tsai, S.B. Liu, I. Wang, Appl. Catal. A 181 (1999) 355.
[2] W.P. Kleinloh, in: Proc. World Petrochem. Conf. (CMAI), Houston, TX, 1997.

[3] (a) G.R. Meima, M.J.M. Van der Aalst, M.S.U. Samson, J.M. Garces, J.G. Lee, in: J. Weitkamp, B. Lücke (Eds.), Proc. DGMK Conf. Catal. Solid Acids and Bases, Berlin, 14–15 March 1996, pp. 125–137;
(b) H. Itoh, T. Hattori, K. Suzuki, Y. Murakami, J. Catal. 79 (1983) 21; PEP Report 33C, SRI International, March 1993.
[4] A. de Angelis, S. Amarilli, D. Derti, L. Montanari, C. Perego, J. Mol. Catal. A: Chem. 146 (1999) 37.
[5] J.M. Valtierra, O. Zaldivar, M.A. Sanchez, J.A. Montoya, J. Navarrete, J.A. de los Reyes, Appl. Catal. A 166 (1998) 387.
[6] J. Panming, W. Qiuying, Z. Chao, X. Yanhe, Appl. Catal. A 91 (1992) 125.
[7] A.B. Halgeri, J. Das, Appl. Catal. A 181 (1999) 347.
[8] N.R. Meshram, S.B. Kulkarni, P. Ratnasawmy, J. Chem. Technol. Biotechnol. 34 (1984) 119.
[9] A. Corma, V.M. Soria, E. Schoeveld, J. Catal. 192 (2000) 163.
[10] D.W. Wojciechowski, Rev. Chem. Intermed. 8 (1987) 21.
[11] D.B. Dadyburjor, A. Bellare, J. Catal. 126 (1990) 261.
[12] S. Siffert, L. Gaillard, B.L. Su, J. Mol. Catal. Chem. 153 (2000) 267.
[13] L.D. Rollmann, D.E. Walsh, J. Catal. 56 (1987) 139.
[14] H.G. Karge, E. Boldingh, Catal. Today 3 (1989) 379.
[15] P. Magnoux, P. Cartraud, S. Mignard, M. Guisnet, J. Catal. 106 (1987) 235.
[16] (a) A.R. Pradhan, B.S. Rao, J. Catal. 132 (1991) 79;
(b) K.S.N. Reddy, B.S. Rao, V.P. Siralkar, Appl. Catal. A 121 (1995) 191.
[17] R.A. Innes, S.I. Zones, G.J. Nacamuli, US patent 4 891 458 (1990).
[18] M. Sasidharan, K.R. Reddy, R. Kumar, J. Catal. 154 (1995) 216.
[19] G. Girotti, F. Rivetti, S. Ramello, L. Carnelli, J. Mol. Catal. A: Chem. 204 (2003) 571.
[20] D. Das, H.K. Mishra, A.K. Dalai, K.M. Parida, Appl. Catal. A 243 (2003) 271.
[21] A. Corma, J.L.G. Fierro, R. Montanana, F. Thomas, J. Mol. Catal. 30 (1985) 361.
[22] E.M. Flanigen, B.M. Lok, R.L. Patton, S.T. Wilson, in: Y. Murakami, A. Iijima, J.W. Ward (Eds.), Proc. 7th Intern. Zeolite Conf., Kodansha, Tokyo, 1986, pp. 103–112.
[23] B.M. Lok, C.A. Messina, R.L. Patton, R.T. Gajek, T.R. Cannan, E.M. Flanigen, J. Am. Chem. Soc. 106 (1984) 6092.
[24] (a) S.P. Elangovan, V. Krishnasamy, V. Murugesan, Catal. Lett. 36 (1996) 271;
(b) H. Nur, H. Hamdan, Mater. Res. Bull. 36 (2001) 315;
(c) G. Lischke, B. Parlitz, U. Lohse, E. Schreier, R. Fricke, Appl. Catal. A 166 (1998) 351.
[25] V.R. Vijayaraghavan, K.J.A. Raj, J. Mol. Catal. A: Chem. 207 (2004) 41, and reference cited therein.
[26] S.K. Saha, S.B. Waghmode, Y. Kubota, Y. Sugi, Mater. Lett. 58 (2004) 2918.
[27] A.T. Hagler, S. Lifson, P. Dauber. J. Am. Chem. Soc. 101 (1979) 5122.
[28] P. Dauber-Osguthorpe, V.A. Roberts, D.J. Osguthorpe, J. Wolff, M. Genest, A.T. Hagler, Proteins: Structure Function Genet. 4 (1988) 31.
[29] S.B. Waghmode, P. Bharathi, S. Sivasanker, R. Vetrivel, Micropor. Mesopor. Mater. 38 (2000) 433, and reference therein.
[30] J.M. Bennett, J.P. Cohen, E.M. Flanigen, J.J. Pluth, J.V. Smith, ACS Symp. Ser. 218 (1983) 109.
[31] R. Deka, R. Vetrivel, Comb. Chem. High Throughput Screening 6 (2003) 1, and reference cited therein.
[32] R. Millini, F. Frigerio, G. Bellussi, P. Giuseppe, P. Giannino, P. Carlo, R.U. Paolo, J. Catal. 217 (2003) 298.
[33] R.F. Lobo, M. Tsapatsis, C.C. Freyhardt, I. Chan, C.-Y. Chen, S.I. Zones, M.E. Davis, J. Am. Chem. Soc. 119 (1977) 3732.
[34] M.H. Zahedi-Niaki, P.N. Joshi, S. Kaliaguine, Chem. Commun. (1996) 1373.
[35] S.B. Waghmode, R. Vetrivel, S.G. Hegde, C.S. Gopinath, S. Sivasanker, J. Phys. Chem. B 107 (2003) 8517.
[36] P. Concepcion, J.M. Lopez Nieto, A. Mifsud, Zeolites 16 (1995) 56.
[37] E.F. Harper, D.Y. Ko, H.K. Lese, E.T. Sabourin, R.C. Willamson, ACS Symp. Ser. 55 (1977) 371.
[38] S.K. Saha, S.B. Waghmode, Y. Kubota, Y. Sugi, Y. Oumi and T. Sano, submitted for publication.